Analysis of Autocatalytic Reactions in Isothermal Catalyst Particles

Multiplicity features of autocatalytic reactions in isothermal catalyst particles with diffusion interaction are presented. Discussed also are two types of autocatalytic reactions—$A + B \rightarrow 2B$ (quadratic) and $A + 2B \rightarrow 3B$ (cubic)—and a decay reaction for autocatalyst B, $B \rightarrow C$, and a nonautocatalytic reaction, $A \rightarrow B$, which generates the autocatalyst. For quadratic reactions, the bifurcation diagrams for a catalyst particle are similar to those for a CSTR. The location of the branch solution, however, is somewhat different. For cubic autocatalytic reactions, the exact parameter regions, where the isola, mushroom, reverse-S, and reverse-S-plus-isola patterns of bifurcation exist, are determined. Furthermore, the parameter space, where a unique solution exists for all Thiele moduli, is also given.

R. Hu
A. V. Sapre
Mobil Research and Development Corporation
Paulsboro, NJ 08066

Introduction

Autocatalytic reactions have been studied extensively for many biochemical reactions involving enzyme systems and only recently in gas phase petrochemical reactions of commercial interest. The feedback mechanism in the reaction kinetics can cause multiple steady states and oscillatory behavior. Gray and Scott (1983, 1984) reported their analysis of autocatalytic reactions in an isothermal CSTR (lumped-parameter system) for the following reaction schemes:

$$\text{Quadratic} \qquad A + \text{B} \rightarrow 2\text{B} \qquad \text{rate} = k_1 ab \tag{1a}$$

$$\text{Cubic} \qquad A + 2B \rightarrow 3B \qquad \text{rate} = k_1 ab^2 \tag{1b}$$

The conversion of A as a function of residence time can show isola and mushroom multiplicity patterns. Recently, Sapre (1988, 1989) showed that these reactions in heterogeneous catalyst particles with diffusion interaction could lead to enhancement in reaction rates and exhibit multiplicity behavior. Such results have been observed experimentally; however, a discussion of experimental data is beyond the scope of this paper. Further mathematical analysis of such complex reaction behaviors is presented here. Hu et al. (1985) found that up to five steady-state solutions exist for a catalytic slab for a first-order exothermic reaction. However, at most only three solutions exist for the same reactions in a CSTR. Thus, the multiplicity patterns due to the interaction between reaction and diffusion could be influenced by the distributed nature of the catalyst.

Theoretical studies of autocatalytic reactions for the Brusselator and Oregonator models, the inorganic chemical oscillators which explain the famous Belousov-Zhabotinski type of reactions are summarized by Nicolis and Prigogine (1977). Additional details on these types of homogeneous reactions, which potentially can generate patterns in time and space, are given by Epstein (1987). Aris and coworkers (1988) recently showed that the simplest chemically and thermodynamically satisfactory model of oscillatory behavior in homogeneous reactions involves only two variables but requires a cubic autocatalator. In this paper we will not discuss the oscillatory behavior of autocatalytic reaction but focus on steady-state bifurcation patterns for heterogeneous autocatalytic systems.

The goal of this study is to determine the multiplicity features of quadratic and cubic autocatalytic reactions in isothermal, catalytic slabs. Additional catalytic or noncatalytic reactions of the following types:

$$A \rightarrow B \qquad \text{rate} = k_a a \tag{2}$$

and a decay reaction for product B

$$B \rightarrow C \qquad \text{rate} = k_d b \tag{3}$$

are also included, as they closely represent the reaction sequence of interest. Recently, Scott (1987), Kaas-Petersen and Scott (1988), and Scott and Farr (1988) added to their earlier CSTR results by studying similar reactions for a distributed parameter system with diffusion of reactants through a permeable boundary. Their results show that reverse-S and reverse-S-plus-isola

patterns exist for cubic autocatalytic reactions. We show here that winged cusp singularity cannot exist for these systems even when nonautocatalytic reactions are introduced, and we present in detail the computational method and accurate parameter values for the reaction network described above.

For complex multiplicity problems, Balakotaiah and Luss (1982, 1984, 1986) have demonstrated that the bifurcation theories are the most useful mathematical tools to predict the multiplicity patterns of various nonlinear algebraic systems. Since the diffusion-reaction interaction is described by two ordinary differential equations (ODE) with split boundary conditions, we will use a shooting method to transform the boundary value problem into two algebraic equations and then analyze its multiplicity features using bifurcation theory. Witmer et al. (1986) were the first to use this technique to find singular points of distributed-parameter systems. Since the two algebraic systems cannot be reduced to a single equation, we also use the Liapunov-Schmidt procedure described by Balakotaiah et al. (1985) to analyze the multiplicity features of a set of algebraic equations.

We start the analysis by considering the case without the $B \rightarrow C$ decay reaction, Eq. 3, and nonautocatalytic $A \rightarrow B$ reaction, Eq. 2. We then extend the analysis by adding the above two reactions and present the global classification of the multiplicity patterns.

Development of Mathematical Model

Consider a kinetic scheme consisting of either Eq. 1a or 1b, and Eqs. 2 and 3 in a single isothermal catalytic slab. The concentrations of reactants A and B satisfy the following differential equations:

$$De_A \frac{d^2a}{dz^2} = k_u a + k_1 a b^n \tag{4}$$

$$De_B \frac{d^2b}{dz^2} = k_d b - k_u a - k_1 a b^n \tag{5}$$

with $n = 1$ or 2 for the quadratic and cubic autocatalytic reaction mechanisms, respectively. The boundary conditions for Eqs. 4 and 5 are:

$$\frac{da}{dz} = 0 \qquad \frac{db}{dz} = 0 \qquad z = 0 \tag{6}$$

$$a = a_o \qquad b = b_o \qquad z = L \tag{7}$$

For simplicity, we will assume that the effective diffusivities of A and B are identical, that is, $De_A = De_B$. We define the following dimensionless variables:

$$\xi = z/L; \quad X_A = a/a_o; \quad X_B = b/a_o;$$
$$\phi^2 = L^2 k_1 a_o^n / De_A; \quad \alpha = k_u/k_1 a_o^n;$$
$$\sigma = b_0/a_o; \quad \delta = k_d/k_1 a_0^n \tag{8}$$

Parameter ϕ is defined as the Thiele modulus of the reaction system. Equations 4–7 are thus transformed to:

$$\frac{d^2X_A}{d\xi^2} = \phi^2 \ (\alpha X_A + X_A X_B^n) \tag{9}$$

$$\frac{d^2X_B}{d\xi^2} = \phi^2 \ (\delta X_B - \alpha X_A - X_A X_B^n) \tag{10}$$

$$\frac{dX_A}{d\xi} = 0 \qquad \frac{dX_B}{d\xi} = 0 \qquad \xi = 0 \tag{11}$$

$$X_A = 1 \qquad X_B = \sigma \qquad \xi = 1 \tag{12}$$

Equations 9–11 can be solved by the shooting method in which the center concentration of A and B, say $t_1 = X_A(0)$ and $t_2 = X_B(0)$, is assumed. Equations 9 and 10 can then be integrated for fixed ϕ^2, σ, δ, and α to check if the outside surface concentration of A and B is satisfied, Eq. 12. If concentrations cannot be matched, then the initial guess is adjusted until the solution is reached. Thus, the problem can be thought of as solving two implicitly defined algebraic equations:

$$\mathbf{F} = \begin{cases} F_1(t_1, t_2, \phi^2, \boldsymbol{p}) = w_1(1, t_2, t_2) - 1 = 0 & (13) \\ F_2(t_1, t_2, \phi^2, \boldsymbol{p}) = w_2(1, t_1, t_2) - \sigma = 0 & (14) \end{cases}$$

where

$$\boldsymbol{p} = (\sigma, \delta, \alpha) \tag{15}$$

and w_1 and w_2 are the solutions to the following initial value problem:

$$\frac{d^2w_1}{d\xi^2} = \phi^2(\alpha w_1 + w_1 w_2^n) = G_1(w_1, w_2, \phi^2) \tag{16}$$

$$\frac{d^2w_2}{d\xi^2} = \phi^2(\delta w_2 - \alpha w_1 - w_1 w_2^n) = G_2(w_1, w_2, \phi^2) \tag{17}$$

$$w_1(0) = t_1 \qquad w_2(0) = t_2 \tag{18}$$

$$\frac{dw_1}{d\xi}(0) = 0 \qquad \frac{dw_2}{d\xi}(0) = 0 \tag{19}$$

We will call t_1 and t_2 the state variables, ϕ^2 the operating variable, and $\mathbf{F}$ the steady state equation. The graph of state variables t_1 or t_2 vs. the operating variable ϕ^2 for a fixed $\boldsymbol{p}$ is called the bifurcation diagram.

The implicit function theorem states that the number of solutions of $\mathbf{F}$ can change only at parameter values satisfying the steady-state Eqs. 13 and 14 and the determinant of the Jacobian matrix of $\mathbf{F}$ equal to zero, that is:

$$\det(\mathbf{L}) = \begin{vmatrix} \dfrac{\partial F_1}{\partial t_1} & \dfrac{\partial F_1}{\partial t_2} \\ \dfrac{\partial F_2}{\partial t_1} & \dfrac{\partial F_2}{\partial t_2} \end{vmatrix} = 0 \tag{20}$$

where $\mathbf{L}$ is the Jacobian matrix of $\mathbf{F}$. We will refer to these solutions as the limit points.

To solve Eq. 20, we need to known the values of $\partial F_i/\partial t_j$. By taking the partial derivatives of F_i with respect to t_j, we get

$$\frac{\partial F_i}{\partial t_j}(t_1, t_2, \phi^2, \boldsymbol{p}) = q_{ij}(1, t_1, t_2) \tag{21}$$

where

$$q_{ij}(\xi, t_1, t_2) = \partial w_i(\xi, t_1, t_2)/\partial t_j \tag{22}$$

The sensitivity functions, $q_{ij}(\xi, t_1, t_2)$, are found by solving the following initial value problem:

$$\frac{d^2q_{11}}{d\xi^2} = \frac{\partial G_1}{\partial w_1} q_{11} + \frac{\partial G_1}{\partial w_2} q_{21} \tag{23}$$

$$\frac{d^2q_{12}}{d\xi^2} = \frac{\partial G_1}{\partial w_1} q_{12} + \frac{\partial G_1}{\partial w_2} q_{22} \tag{24}$$

$$\frac{d^2q_{21}}{d\xi^2} = \frac{\partial G_2}{\partial w_1} q_{11} + \frac{\partial G_2}{\partial w_2} q_{21} \tag{25}$$

$$\frac{d^2q_{22}}{d\xi^2} = \frac{\partial G_2}{\partial w_1} q_{12} + \frac{\partial G_2}{\partial w_2} q_{22} \tag{26}$$

The corresponding initial conditions are:

$$q_{11}(0) = q_{22}(0) = 1 \qquad q_{12}(0) = q_{21}(0) = 0 \tag{27}$$

$$\frac{dq_{11}}{d\xi}(0) = \frac{dq_{12}}{d\xi}(0) = \frac{dq_{21}}{d\xi}(0) = \frac{dq_{22}}{d\xi}(0) = 0 \tag{28}$$

The limit points can be calculated by guessing the three values of t_1, t_2, and ϕ^2 for a fixed value of $\boldsymbol{p}$. The resulting initial value problem—Eqs. 16, 17, and 23–26—can then be integrated from the center of the pellet ($\xi = 0$) using the Runge-Kutta method. The three algebraic equations, Eqs. 13, 14, and 20, are solved by the Newton-Raphson method. The required Jacobian matrix is generated numerically.

For the case without the decay reaction, $\delta = 0$, Eqs. 9 and 10 can be simplified to:

$$\frac{d^2X_A}{d\xi^2} = \phi^2[\alpha X_A + X_A(1 + \sigma - X_A)^n] = G_3(X_A, \phi^2) \tag{29}$$

Thus the system of equations is reduced to a single algebraic equation F_1 in one unknown t_1. From Eq. 20 we know that the limit point can be calculated by solving Eq. 13 and the following equation:

$$\frac{\partial F_1}{\partial t_1} = q_{11}(1, t_1) = 0 \tag{30}$$

$w_1(\xi)$ and $q_{11}(\xi)$ can then be calculated by solving the following initial value problem:

$$\frac{d^2w_1}{d\xi^2} = G_3(w_1, \phi^2) \tag{31}$$

$$\frac{d^2q_{11}}{d\xi^2} = \frac{\partial G_3}{\partial w_1} q_{11} \tag{32}$$

with the initial conditions defined by Eqs. 18, 19, 27, and 28.

Results and Discussion

Quadratic autocatalytic reactions ($n = 1$)

1. Without Decay Reaction ($\delta = 0$). Let us first consider the simplest case in which species B, the autocatalytic agent, does not exist at the catalyst surface, that is, $\sigma = 0$. Also, the $A \rightarrow B$ reaction has no influence ($\alpha = 0$). This situation represents, for example, the entrance region of a packed bed reactor. Equation 29 thus becomes:

$$\frac{d^2X_A}{d\xi^2} = \phi^2 X_A(1 - X_A) \tag{33}$$

By solving Eq. 33 with boundary conditions as in Eqs. 11 and 12, the bifurcation diagram of t_1 vs. ϕ^2 is generated. This is graphically shown in Figure 1. There are two branches to the solution. The first is the trivial solution, $X_A(\xi) = 1$ and $X_B(\xi) = 0$ for all ϕ^2, and corresponds to a no-reaction case. The second branch solution corresponds to the case in which the initial concentration of B inside the catalyst is not zero. When ϕ^2 is large, the reaction is fast enough to overcome the loss of B by diffusion and the species B does not "wash away." When ϕ^2 decreases, $X_B(0) = 1 - X_A(0)$ decreases to zero at point A. It is shown in Appendix A that the value of ϕ^2 at point A is equal to $\Pi^2/4$. For smaller values of ϕ^2, the reaction rate is slower than the diffusion rate and only the trivial solutions exist.

When there is a small amount of B, the autocatalytic agent, at the catalyst surface ($\sigma > 0$), the trivial solution branch disappears. The concentration of A at the center of the catalyst then decreases monotonically from unity to zero with increasing ϕ^2. Figure 2 shows the bifurcation diagram of $X_A(0)$ vs. ϕ^2 for $\sigma = 0.1$. Similarly, if the nonautocatalytic reaction ($\alpha > 0$) contributes to the formation of B, the same phenomenon occurs. Figure 3 shows the bifurcation diagram of $X_A(0)$ vs. ϕ^2 for $\alpha = 0.01$.

2. With Decay Reaction ($\delta > 0$). The behavior of a quadratic autocatalytic reaction with $B \rightarrow C$ decay reaction is similar to the above example without the decay reaction. When both σ and α are equal to zero, the bifurcation diagram is similar to Figure 1; however, the value of ϕ^2 for point A is different when $\delta = 0$. It is shown in Appendix A that the value of ϕ^2 is equal to $\Pi^2/4(1 - \delta)$ for $\delta < 1$. When $\delta \geq 1$, the decay reaction is faster than

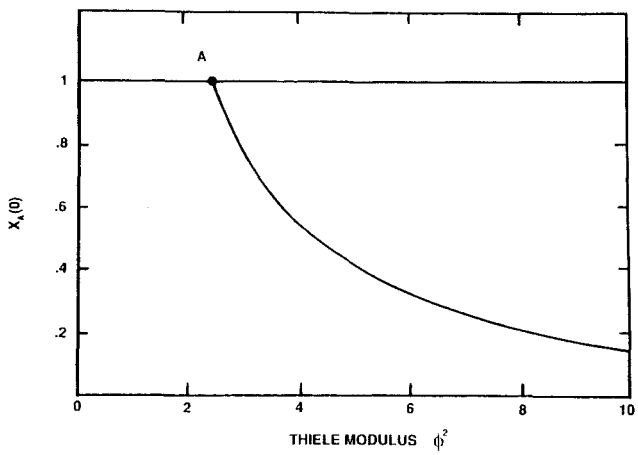

Figure 1. Bifurcation diagram for quadratic autocatalytic reactions, $\delta = \alpha = \sigma = 0$.

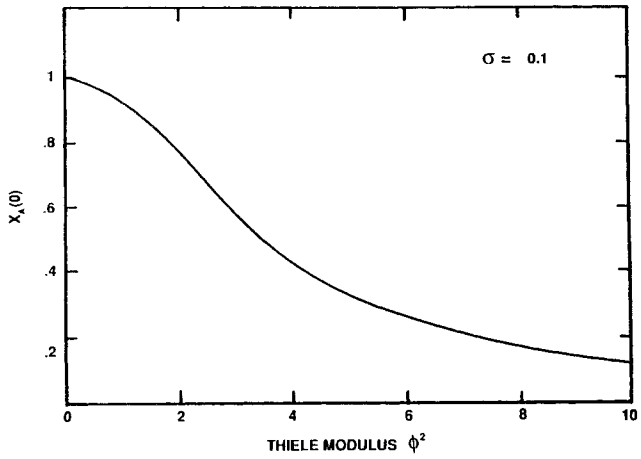

Figure 2. Bifurcation diagram for quadratic autocatalytic reactions, $\delta = \alpha = 0$, $\sigma = 0.1$.

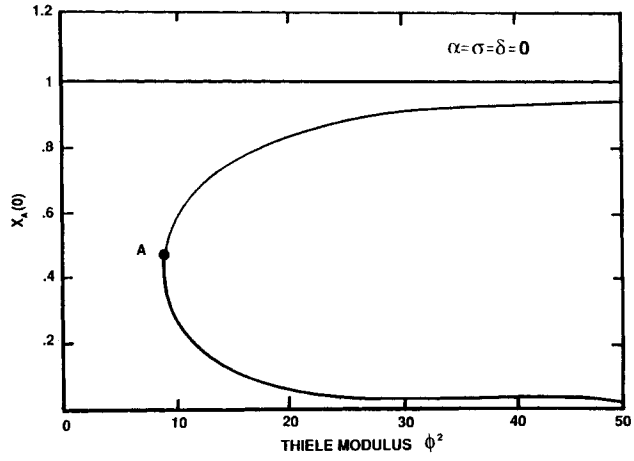

Figure 4. Bifurcation diagram for cubic autocatalytic reactions, $\delta = \sigma = \alpha = 0$.

the autocatalytic reaction and species B is exhausted inside the catalyst. Only the trivial solutions exist for $\delta \geq 1$. For the case of $\sigma > 0$ and $\alpha > 0$, the bifurcation diagrams are similar to Figures 2 and 3.

Cubic autocatalytic reactions ($n = 2$)

1. Without Decay Reaction ($\delta = 0$). As before, we start the analysis by examining the case for which $\alpha = 0$ and $\sigma = 0$. The bifurcation diagram of $X_A(0)$ vs. ϕ^2 is shown in Figure 4. There are three different branches of solutions and a single limit point A. The first branch corresponds to the no-reaction case. It can be shown that the intermediate branch of solution is always unstable. If we start the experiment with a small amount of B inside the catalyst, the concentration of A will stay in the lower branch for large ϕ^2. By decreasing the value of ϕ^2, the concentration of A increased gradually until point A. At limit point A, autocatalyst B is washed away and reaction extinguishes. The exact coordinate of point A can be calculated by solving Eqs. 13 and 30 simultaneously, which gives $\phi^2 = 10.2881$ and $X_A(0) = 0.4313$ at point A. For ϕ^2 smaller than that of point A, only the no-reaction case can exist.

The presence of autocatalyst B at the catalyst surface results in an additional limit point on the bifurcation diagram, and for this case a complete hysteresis loop is exhibited. The bifurcation diagram for $\sigma = 0.02$ is shown in Figure 5. For values of ϕ^2 larger than that of point C, only the high conversion state can exist. By decreasing ϕ^2 below that of point A, reaction extinguishes to the low conversion state, that is, almost no conversion. On the other hand, with increasing ϕ^2 the reaction will stay in the low conversion state until the ignition point C. At point C, the reaction will jump to the high conversion state. Therefore, there are two stable and one unstable steady-state solutions for ϕ^2 between points A and C.

Plotting the value of ϕ^2 for points A and C as a function of σ, we get the locus of the limit points as shown in Figure 6. The locus of the extinction point (line AB) and ignition point (line BC) emerges as a cusp from point B. For the parameters inside cusp ABC, three solutions exist. A unique solution exists only for the parameters outside the cusp. Point B is called the cusp point. The exact coordinate of the cusp point for a single algebraic equation $F_1(t_1) = 0$ can be calculated by solving (Balakotaiah and Luss, 1984):

$$F_1 = \frac{\partial F_1}{\partial t_1} = \frac{\partial^2 F_1}{\partial t_1^2} \tag{34}$$

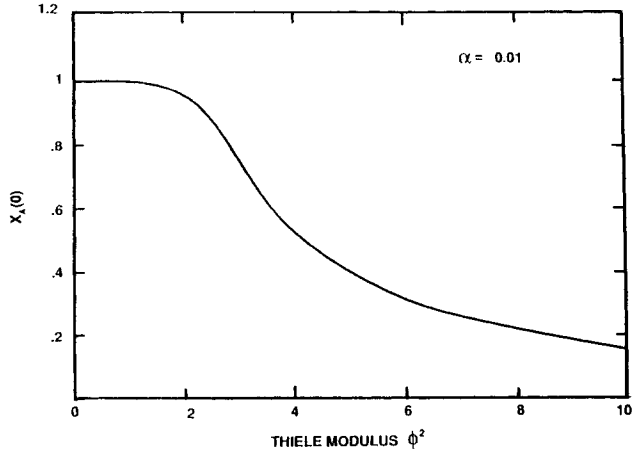

Figure 3. Bifurcation diagram for quadratic autocatalytic reactions, $\delta = \alpha = 0$, $\sigma = 0.01$.

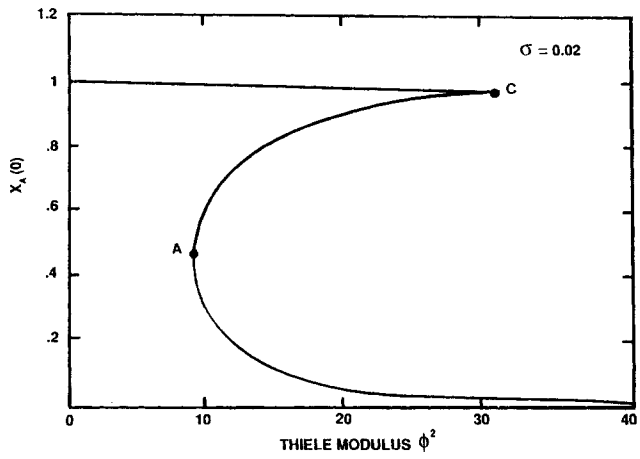

Figure 5. Bifurcation diagram for cubic autocatalytic reactions, $\delta = \alpha = 0$, $\sigma = 0.02$.

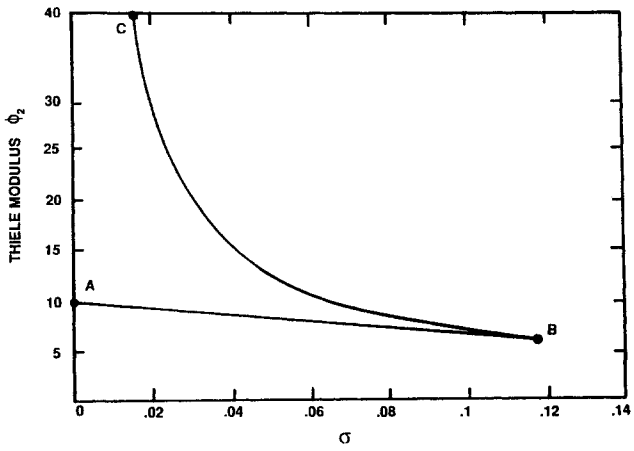

Figure 6. Locus of limit points for cubic autocatalytic reactions in (ϕ^2, σ) plane, $\delta = \alpha = 0$.
Three solutions exist for the parameters inside the cusp *ABC*

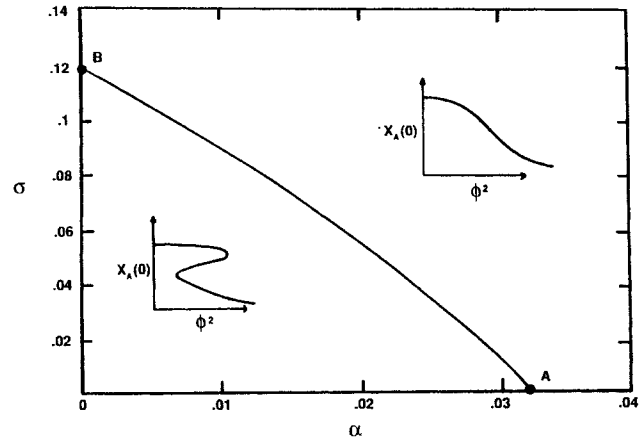

Figure 7. Hysteresis variety for cubic autocatalytic reactions in the (σ, α) plane with no decay reaction.
Insets: corresponding bifurcation diagrams

Substituting Eq. 13 into Eq. 34, we get

$$\frac{\partial^2 F_1}{\partial t_1^2} = q_{111}(1, t_1) = 0 \tag{35}$$

where $q_{111}(\xi,t_1) = \partial^2 w_1(\xi, t_1)/\partial t_1^2$. q_{111} is obtained by solving the following initial value problem:

$$\frac{d^2 q_{111}}{d\xi^2} = \frac{\partial^2 G_3}{\partial w_1^2} q_{11}^2 + \frac{\partial G_3}{\partial w_1} q_{111} \tag{36}$$

$$q_{111}(0) = 0, \qquad dq_{111}(0)/d\xi = 0$$

Thus, the exact coordinate of point B can be calculated by first guessing values of $X_A(0)$, ϕ^2, and σ. The initial value problem described by Eqs. 31, 32, and 36 is then integrated from $\xi = 0$ to $\xi = 1$. The three algebraic equations, Eqs. 13, 30, and 35 are then solved by the Newton-Raphson method. The unique coordinate values of σ, ϕ^2, and $X_A(0)$ for point B are 0.1186, 6.0242, and 0.7127, respectively.

The bifurcation diagram, and the locus of the limit point for the case that includes nonautocatalytic conversion of A ($\alpha \neq 0$), are similar to Figures 5 and 6, but the coordinates of point B are now a function of α and σ. The value of σ for the cusp point B as a function of α are plotted in Figure 7. The locus of the cusp point is called the hysteresis variety (Balakotaiah and Luss, 1984). For the parameters inside this variety, the bifurcation diagram is a reverse-S-shape diagram, and multiple solutions exist for some values of ϕ^2. For the parameters outside this variety, the bifurcation diagram is a monotonic curve, and a unique solution exists for all ϕ^2. Thus, the hysteresis variety is also the uniqueness boundary. From Figure 7, we also see that when there is no autocatalyst B in the surrounding ($\sigma = 0$), multiplicity disappears when the ratio of nonautocatalytic reaction rate to autocatalytic reaction rate exceeds 0.0318.

2. With Decay Reaction ($\delta \neq 0$). We will use the global mapping technique described by Balakotaiah and Luss (1984) to analyze this case. This technique involves finding first the most degenerated singular point, then separating the global parameter regions into regions with different bifurcation diagrams. Since steady-state Eqs. 13 and 14 contain four parameters (ϕ^2, σ, δ, α) and as a winged cusp singular point is known to exist for at least the lumped system (Gray and Scott, 1984), we will assume that the highest singular point is a winged cusp point for our problem. For a single algebraic system $f(t, \phi^2, p) = 0$, this point has properties such that the following conditions are satisfied:

$$f = \frac{\partial f}{\partial t} = \frac{\partial^2 f}{\partial t^2} = \frac{\partial f}{\partial(\phi^2)} = \frac{\partial^2 f}{\partial t \partial(\phi^2)} = 0 \tag{37}$$

Unfortunately, Eqs. 9 and 10 cannot be simplified to a single differential equation for $\delta \neq 0$. Therefore, we use the Liapunov-Schmidt method for a set of algebraic equations as proposed in the literature (Golubitsky and Keyfitz, 1980). The Liapunov-Schmidt (L-S) reduction method is a procedure to reduce a system of N algebraic equations with N state variables to a set of n algebraic equations with n state variables when the rank of the matrix $\mathbf{L} = (dF)$ is r ($r = N - n$) with $1 \leq r \leq N - 1$. It can be shown that the rank of Jacobian matrix $\mathbf{L}$, Eq. 20, is always larger than one. Thus, according to the implicit function theory, the state variable t_2 can be expressed as an implicit function of t_1, and the system is said to have only one intrinsic state variable. Based on the L-S reduction procedure, Eqs. 13–14 can be reduced to one algebraic equation:

$$F_1(t_1, t_2(t_1), \phi^2, p) = 0 \rightarrow f(t_1, \phi^2, p) = 0 \tag{38}$$

Equation 38 is called the branching equation.

The formula for calculating the first derivative of f with respect to t_1 is the determinant of the Jacobian matrix of F. The $\partial f/\partial t_1 = 0$ is equivalent to Eq. 20. This leads to the following identity:

$$q_{11}(1)q_{22}(1) - q_{12}(1)q_{21}(1) = 0 \tag{39}$$

Similarly, the second derivative can also be calculated using the previously described method (Balakotaiah et al. 1985):

$$f_{tt} = \langle v, d^2\mathbf{F}(u, u)\rangle \tag{40}$$

Where $\langle u, v\rangle$ is the inner product of vectors u and v, and u and v

are the eigenvectors and eigenrows of Jacobian matrix L, with zero eigenvalue, respectively.

The kth differential of the branching equation f with respect to the state variable is defined by:

$$(d^k\mathbf{F})(w^1, w^2, \ldots w^k) = \sum_{\alpha_1=1}^{N}\sum_{\alpha_2=1}^{N}\cdots\sum_{\alpha_k=1}^{N} \frac{\partial^k F}{\partial x_{\alpha_1}\partial x_{\alpha_2}\ldots\partial x_{\alpha_k}} w^1_{\alpha_1}\ldots w^k_{\alpha_k} \quad (41)$$

where $x_{\alpha j}$ and $w^1_{\alpha j}$ are the α_jth components of the N-dimensional vector x and w^1, respectively. Substituting Eqs. 13 and 14 into Eqs. 40 and 41, for $\partial^2 f/\partial t^2 = 0$ we get

$$u = [q_{22}(1), -q_{21}(1)]^T, \quad v = [q_{22}(1), -q_{12}(1)]$$

$$d^2\mathbf{F}(u,u) = \begin{bmatrix} q_{111}(1)q_{22}^2(1) - 2q_{112}(1)q_{22}(1)q_{21}(1) \\ \quad + q_{122}(1)q_{21}^2(1) \\ q_{211}(1)q_{22}^2(1) - 2q_{212}(1)q_{22}(1)q_{21}(1) \\ \quad + q_{222}(1)q_{21}^2(1) \end{bmatrix} = \begin{pmatrix} \epsilon_1 \\ \epsilon_2 \end{pmatrix} \quad (42)$$

$$f_{tt} = \epsilon_1 q_{22}(1) - \epsilon_2 q_{12}(1) = 0 \quad (43)$$

where

$$q_{ijk} = \partial^2 w_i(\xi, t_1, t_2)/\partial t_j \partial t_k \quad (44)$$

The sensitivity functions q_{ijk} can be obtained by solving the initial value problem, Eqs. B1–B5, as shown in Appendix B.

The first derivative of branching equation f with respect to ϕ^2 is given as:

$$f_{\phi^2} = \langle v, \mathbf{F}_{\phi^2}\rangle \quad (45)$$

where

$$\mathbf{F}_{\phi^2} = (\partial F_1/\partial\phi^2, \partial F_2/\partial\phi^2, \text{— — —}, \partial F_N/\partial\phi^2)^T \quad (46)$$

Substitution of Eqs. 13 and 14 into Eqs. 45 and 46 produces

$$f_{\phi^2} = q_{22}(1)q_{13}(1) - q_{12}(1)q_{23}(1) = 0 \quad (47)$$

where

$$q_{i3}(\xi) = \partial w_i(\xi, \phi^2, t_1, t_2)/\partial\phi^2 \quad (48)$$

The sensitivity function $q_{i3}(\xi)$ can be obtained by solving the initial value problem described by Eqs. B6–B8.

The second derivative of f with respect to t and ϕ^2 can then be calculated,

$$f_{t\phi^2} = \langle v, dF_{\phi^2}\cdot u - d^2F(u, z^1)\rangle \quad (49)$$

where the matrix

$$dF_{\phi^2} = \left[\frac{\partial^2 F_i}{\partial t_j \partial\phi^2}\right]_{ij} \quad (50)$$

and the vector z^1 are given by the linear equations

$$\mathbf{L}z^1 + \mathbf{E}F_{\phi^2} = 0 \quad (51)$$

where $\mathbf{E}$ is the projection operator onto the range of $\mathbf{L}$

$$\mathbf{E} = \mathbf{I} - \frac{vv^T}{\langle v, v\rangle} \quad (52)$$

Substituting Eqs. 13 and 14 into Eqs. 49–52, we get

$$z^1 = \begin{bmatrix} cq_{21}(1) \\ cq_{22}(1) \end{bmatrix} = \begin{bmatrix} \epsilon_3 \\ \epsilon_4 \end{bmatrix} \quad (53)$$

where

$$c = \frac{q_{22}(1)\,[q_{12}(1)q_{13}(1) + q_{22}(1)q_{23}(1)]}{[(q_{21}(1)^2 + q_{22}(1)^2)\,(q_{22}(1)^2 + q_{12}(1)^2)]} \quad (54)$$

$$d^2\mathbf{F}(u, z^1) = \begin{bmatrix} q_{111}(1)q_{22}(1)\epsilon_3 + q_{112}(1)[q_{22}(1)\epsilon_4 - q_{21}(1)\epsilon_3] \\ \quad - q_{122}(1)q_{21}(1)\epsilon_4 \\ q_{211}(1)q_{22}(1)\epsilon_3 + q_{212}(1)[q_{22}(1)\epsilon_4 - q_{21}(1)\epsilon_3] \\ \quad - q_{222}(1)q_{21}(1)\epsilon_4 \end{bmatrix} = \begin{pmatrix} \epsilon_5 \\ \epsilon_6 \end{pmatrix} \quad (55)$$

$$f_{t\phi^2} = q_{22}(1)[q_{113}(1)q_{22}(1) - q_{123}(1)q_{21}(1) - \epsilon_5] - q_{12}(1)[q_{213}(1)q_{22}(1) - q_{223}(1)q_{21}(1) - \epsilon_6] = 0 \quad (56)$$

where $q_{ij3}(\xi) = \partial^2 w_i(\xi, t_1, t_2, \phi^2)/\partial t_j \partial\phi^2$. The sensitivity functions q_{ij3} is calculated by solving the initial value problem described by Eqs. B9–B10.

The numerical method of solving the winged cusp point involves guessing values for six parameters: t_1, t_2, ϕ^2, σ, δ, and α. The resulting eighteen initial value problems (Eqs. 16, 19, 23–26, B1–B3, B6, and B9) are then integrated from $\xi = 0$ to $\xi = 1$. The resulting six algebraic equations (Eqs. 13, 14, 39, 43, 47, and 56) are then solved by the standard Newton-Raphson method.

The exact coordinates of the winged cusp point are

$$X_A(0) = 0.7077; \quad X_B(0) = 0.1933; \quad \phi^2 = 23.8106; \quad \sigma = 0.1217; \quad \delta = 0.1026; \quad \alpha = \alpha_0 = -0.0001055 \quad (57)$$

Since the parameter α is outside the feasible parameter range, this winged cusp singular point cannot exist in real space. From the singularity theory (Golubitsky and Keyfitz, 1980), we also know that Eqs. 13 and 14 are equivalent to the polynomial:

$$x^3 - \lambda^2 + \gamma_1 + \gamma_2\lambda + \gamma_3 x\lambda = 0 \quad (58)$$

in the vicinity of the winged cusp singular point. Here x and λ are equivalent to $1 - t$ and ϕ^2, respectively. Seven different kinds of bifurcation diagrams are produced when $\gamma_i \neq 0$, Figure 8. For the same reaction system in a CSTR, winged cusp singu-

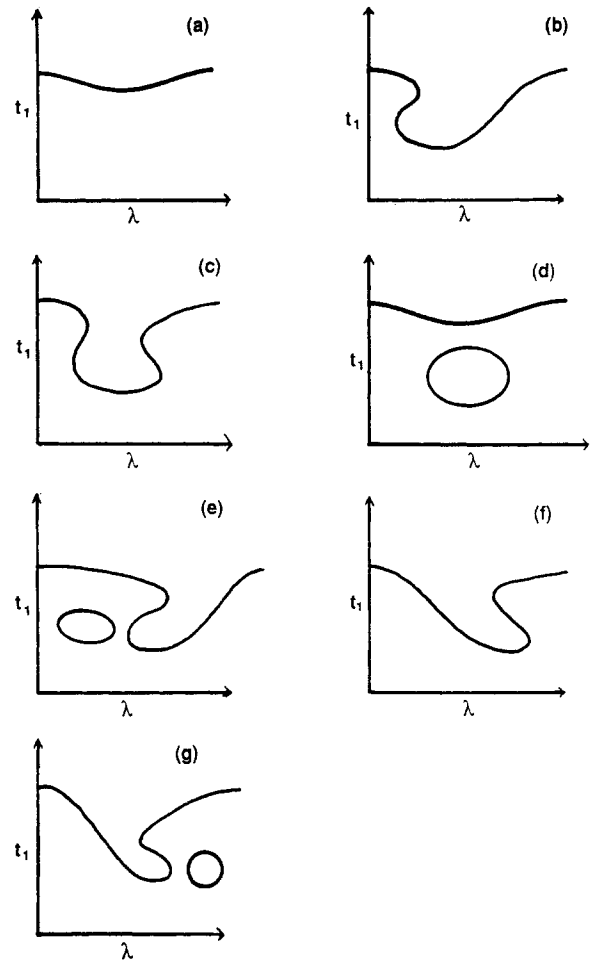

Figure 8. The seven bifurcation diagrams patterns for a winged-cusp singularity.

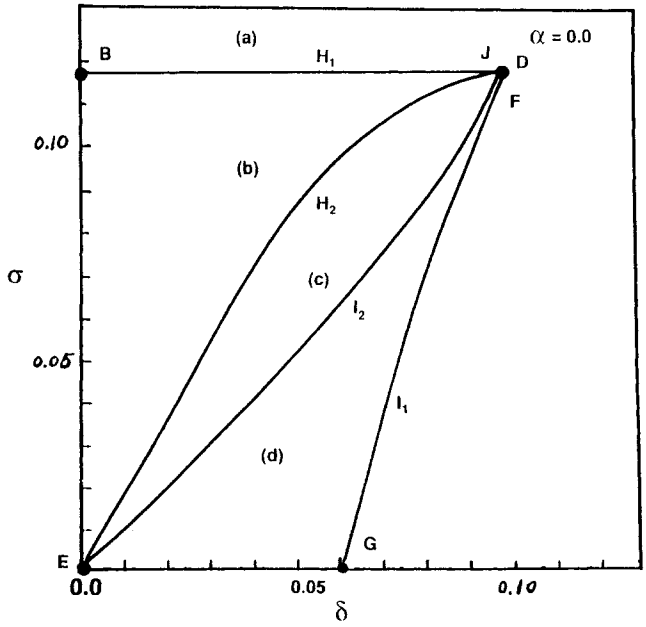

Figure 9. Cross section of hysteresis and isola varieties for cubic autocatalytic reactions in the (σ, δ) plane, $\alpha = 0$.

larity was shown at $\alpha = 0$ (Gray and Scott, 1984). Perturbation around the singular point would degenerate Figure 8b to Figure 8e. Similarly, Figure 8f would lead to Figure 8g. However, both of these pairs will exist in the opposite direction from each other near the singular point (i.e., $\alpha > \alpha_0$ or $\alpha < \alpha_0$). Since the bifurcation diagram of Figure 8b exists for the case without the decay reaction ($\delta = 0$), and for feasible solutions $\alpha > 0$; then Figures 8a–e are the only feasible solutions. The bifurcation diagrams of Figures 8f and 8g exist only when $\alpha < 0$ and therefore are not feasible.

The exact parameter regions for which these bifurcation diagrams exist can be determined by constructing the hysteresis variety and the isola variety (Balakotaiah and Luss, 1982). When the parameter crosses the hysteresis variety, two limit points appear or disappear, so that the bifurcation diagram changes from a monotonic shape to an S or an inverse-S shape, Figure 8a to 8b. The hysteresis variety can be determined by solving Eq. 34. When the parameter crosses the isola variety, typically two limit points appear or disappear, so that either the bifurcation diagram separates locally into two isolated curves, Figure 8c to 8d, or one of the isolated curves disappears, Figure 8e to 8b. The isola variety is obtained by eliminating t and ϕ^2 from

$$f = \frac{\partial f}{\partial t} = \frac{\partial f}{\partial(\phi^2)} \tag{59}$$

The hysteresis and isola varieties are surfaces in three-dimensional space of σ, δ, and α. Since it is difficult to construct a three-dimensional plot, we construct two-dimensional cross sections of the hysteresis variety in the (σ, δ) plane for various fixed values of α. For a fixed value of α, the hysteresis variety can be obtained by solving Eqs. 13, 14, 39, and 43 for $X_A(0)$, $X_B(0)$, ϕ^2, and σ by varying the value of δ. For $\alpha = 0$, the hysteresis variety can be obtained by starting from point B in Figure 6, that is, $\alpha = 0$ and $\delta = 0$. The hysteresis variety is shown as curves $BD(H_1)$ and $DE(H_2)$ in Figures 9 and 10. The hysteresis variety has a turning point at point D. The slope of the hysteresis variety at point D is infinity. Thus, the coordinate of point D can be calculated by solving Eq. 34 and

$$\frac{\partial^2 f}{\partial t \partial \sigma}\frac{\partial f}{\partial \phi^2} - \frac{\partial f}{\partial \sigma}\frac{\partial^2 f}{\partial t \partial \phi^2} = 0 \tag{60}$$

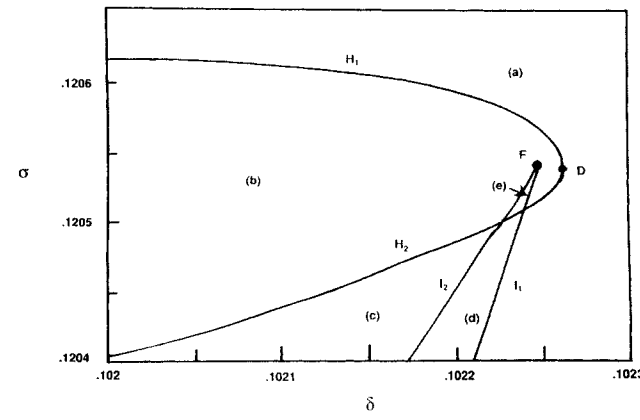

Figure 10. Detail diagram of the region close to point D, Figure 9.

The exact coordinates for point D are then

$$\delta = 0.102268 \equiv \delta_D; \quad \sigma = 0.12054 \tag{61}$$

For $\delta > \delta_D$ the hysteresis variety ceases to exist. When the parameter crosses H_1 from region (a) to region (b), a multiplicity region appears at low ϕ^2 and the bifurcation diagram changes from a monotonic curve to a curve with an inverse-S shape, Figure 8. When the parameter crosses H_2 from region (b) to region (c), another multiplicity region appears at high ϕ^2 and the bifurcation diagram changes from an inverse-S shape to an inverse mushroom shape, Figure 8. The isola variety is obtained by solving Eqs. 13, 14, 39, and 47 for a fixed δ. The isola variety emanates as a cusp from point F, Figures 9 and 10. One branch of solutions goes to point E, at which $\delta = \sigma = 0, X_A(0) = 1$, and $\phi^2 = \infty$. The second branch of solutions goes to point G, at which $\sigma = 0, \delta = 0.0600, X_A(0) = 0.4331$, and $\phi^2 = 41.213$. The exact coordinates of point F can be calculated by solving Eq. 59 and

$$\frac{\partial^2 f}{\partial t^2}\frac{\partial^2 f}{\partial (\phi^2)^2} - \left(\frac{\partial^2 f}{\partial t \partial \phi^2}\right)^2 = 0 \tag{62}$$

The exact coordinates for point F are

$$\delta = 0.10225 \equiv \delta_F; \quad \sigma = 0.120536 \equiv \sigma_F \tag{63}$$

When the parameter crosses I_2 from region (c) to region (d), the resulting two limit points in the neck of the mushroom connect with each other and an isolated curve exists at lower values of t, Figure 8d. When the parameter crosses I_1 from region (d) to region (a), the isolated curve shrinks to a point and disappears. The hysteresis variety and isola variety separate the σ vs. δ plane into five regions. The bifurcation diagrams corresponding to regions (a), (b), (c), and (d) are shown in Figure 11a, b, c, and d, respectively. The parameter region for region (e) is too small to show the isola and the limit point in this figure. Thus, we only show the schematic plot of the bifurcation diagram in Figure 8e. From Figures 9 and 10, we know a unique solution exists for any Thiele modulus when $\delta > \delta_D$ and $\sigma > 0.120635 \equiv \sigma_J$ (point J). At point J, the slope of the hysteresis variety H_1 is equal to zero. Thus, the coordinates of point J can be calculated by solving Eq. 34 and

$$\frac{\partial^2 f}{\partial t \partial \delta}\frac{\partial f}{\partial \phi^2} - \frac{\partial f}{\partial \delta}\frac{\partial^2 f}{\partial t \partial \phi^2} = 0 \tag{64}$$

The exact coordinates for point J are

$$\delta = 0.1015; \quad \sigma = 0.120635 \equiv \sigma_J \tag{65}$$

Table 1 reports the values of the parameters of some important points in Figures 7, 9, and 10.

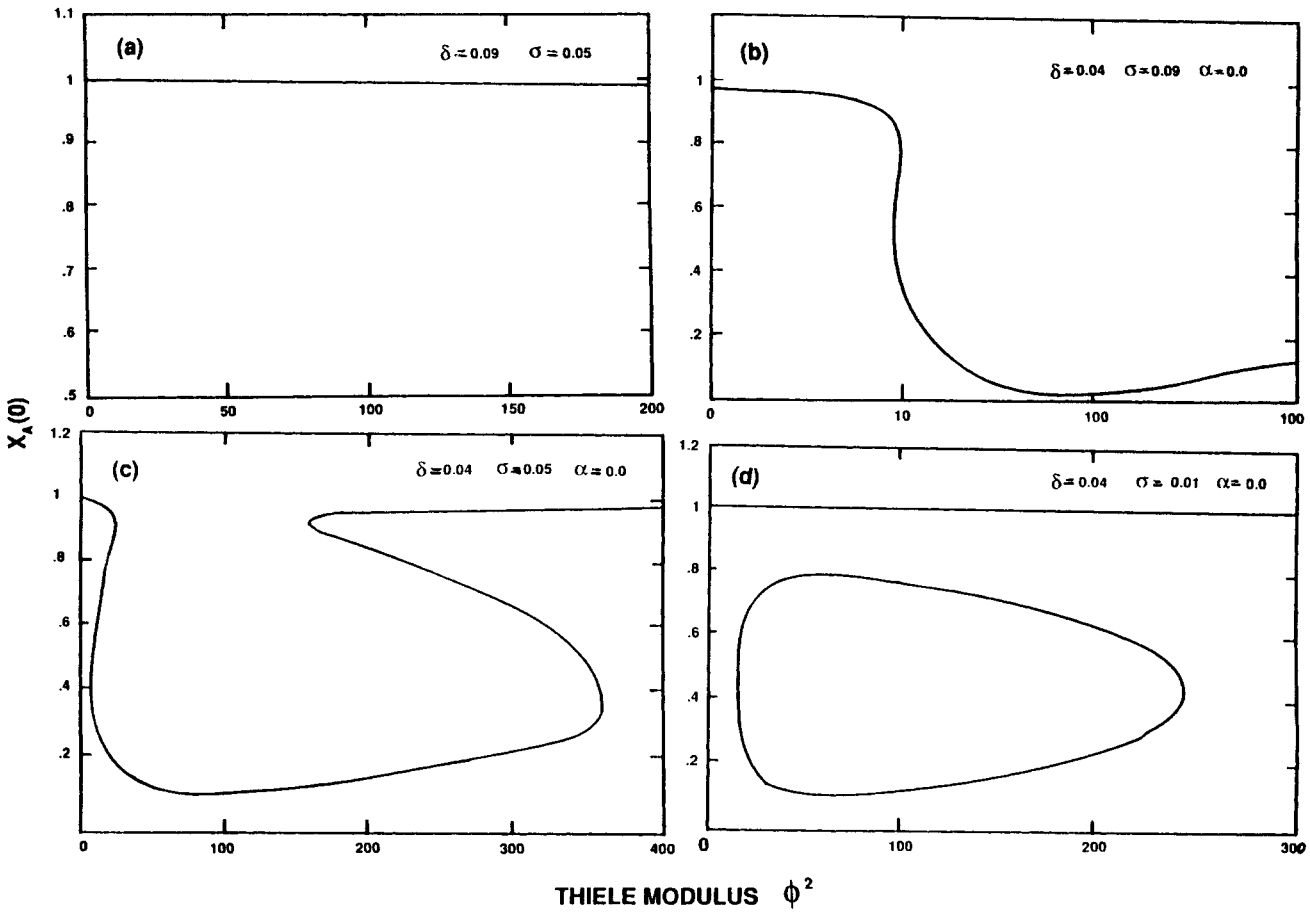

Figure 11. Bifurcation diagram for cubic autocatalytic reactions with different δ, σ, and α values.
(a), (b), (c), (d) correspond to parameter values in regions (a), (b), (c), (d) in Figure 9.

Table 1. Parameter Values of Some Points on the Hysteresis and Isola Varieties Shown in Figures 7, 9, and 10

Parameter	Point						
	A	*B*	*D*	*E*	*F*	*G*	*J*
δ	0	0	0.10227	0	0.10225	0.0600	0.1015
σ	0	0.1186	0.120540	0	0.120536	0	0.120635
α	0.0318	0	0	0	0	0	0
ϕ^2	8.541	6.0242	23.5678	∞	24.0400	41.2130	20.1780
$X_A(0)$	0.6243	0.7127	0.7070	1	0.7072	0.4331	0.7081

For $\alpha = 0.0025$, the hysteresis variety and isola variety are shown in Figure 12. The value of σ for hysteresis variety H_1 decreases monotonically with increasing δ until point D. Thus, multiplicity exists for some values of ϕ^2 if $\sigma < \sigma_B = 0.11133$. The value of δ for hysteresis variety H_2 decreases monotonically with decreasing σ. Thus, multiplicity exists for some values of ϕ^2, if $\delta < \delta_D = 0.09488$. Point E_1 does not end at origin. Thus, there exists an inverse-S-shape pattern for the case of no autocatalyst at the catalyst surface. The isola variety emanates as a cusp at point F. The vicinity of cusp point F is similar to that of Figure 10. There is a small triangular region (e) surrounded by hysteresis and isola varieties. The value of δ at point E_2 is larger than that of point E_1. Thus, region (c) inside which the bifurcation diagram is an inverse mushroom still exists but is rather small. The bifurcation diagrams in each of the regions are similar to the bifurcation diagrams for $\alpha = 0$. When α increases, the value of σ at point F decreases, and points E_2 and G come close together. Finally, at $\alpha = 0.0042717$, regions (c), (d) and (e) disappear and isola variety ceases to exist. The value of σ for point B decreases with increasing α, while the value of δ for point E_1 first increases then decreases with increasing α. Figure 13 shows the hysteresis variety and multiplicity region for $\alpha = 0.01$. The region shrinks with increasing α. Points B and E_1 go to the origin and region (b) disappears at $\alpha = 0.0318$ ($\sigma = 0$ in Figure 7).

By using the global mapping technique, we determined the exact parameter regions for each patterns of the bifurcation diagram. We also determined the maximum values of α, σ, and δ for which multiplicity can exist for some ϕ^2. The values are 0.0318, 0.120635 and 0.102268, respectively.

Several models studied in the previous sections involve rather simple reactions in an isothermal catalyst particle. Despite the simplicity, a remarkable array of complex behavior can arise because of the interaction of diffusion with nonlinear autocatalytic reactions. Other than the work of Scott et al. referred to before, we have not come across such exotic behavior for such simple reactions. Scott also studied the dynamic behavior of similar systems and showed that sustained oscillations are possible.

Conclusions

The multiplicity features of the quadratic autocatalytic reactions inside an isothermal catalytic slab are similar to the same reactions in a CSTR. The trivial solution is eliminated by intro-

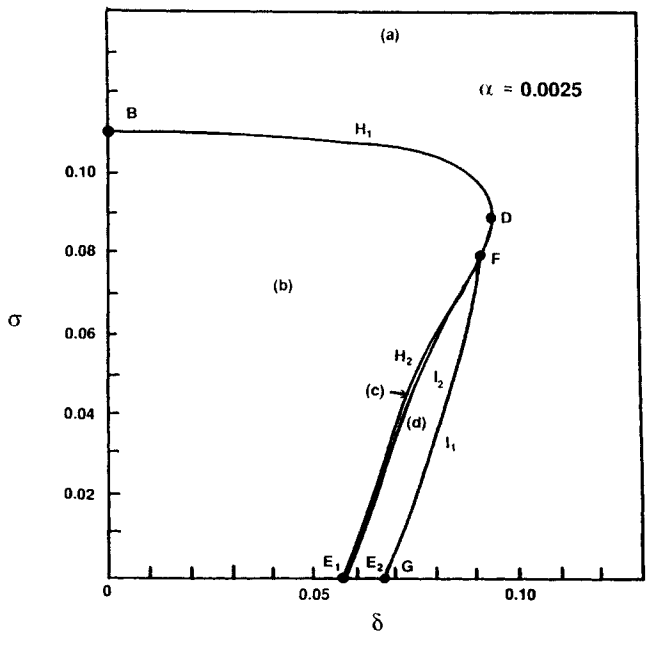

Figure 12. Cross section of hysteresis and isola varieties for cubic autocatalytic reactions in the (σ, δ) plane, $\alpha = 0.0025$.

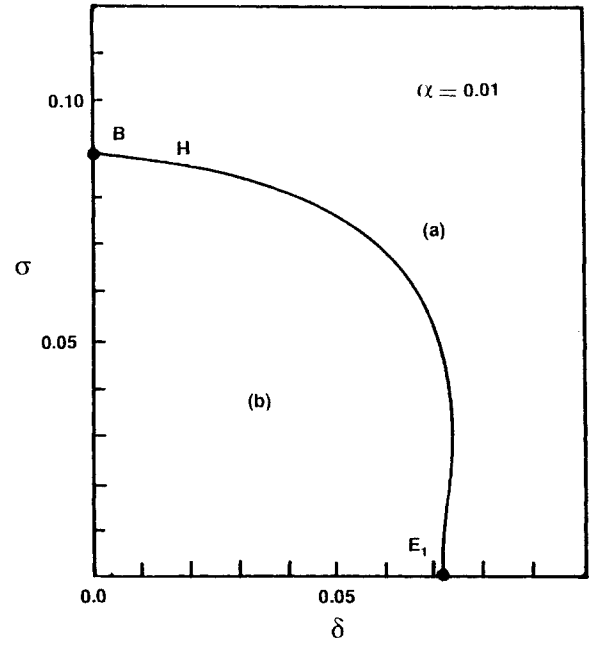

Figure 13. Cross section of hysteresis variety for cubic autocatalytic reactions in the (σ, δ) plane, $\alpha = 0.01$.

ducing either the autocatalyst B at the surface of the catalyst or the nonautocatalytic reaction producing B from A.

Five different patterns of bifurcation diagrams are found for the cubic autocatalytic reactions with a decay reaction of the autocatalyst in an isothermal catalyst slab, compared to three in a CSTR. Reverse-S and reverse-S-plus-isola patterns exist besides the mushroom and isola patterns. Introducing the nonautocatalytic reaction does not give the higher degenerate forms of singularity, that is, the winged-cusp singularity. Thus, the number of patterns for bifurcation diagrams does not change when the reaction rate of nonautocatalytic reaction changes. However, the regions at which isola and mushroom multiplicities exist shrink and finally disappear from the feasible parameter regions. The uniqueness region for all Thiele moduli is determined by constructing the hysteresis variety and isola variety. The analysis shows that a unique solution exists if the ratio of the concentrations of autocatalyst B to reactant A at the surface of the catalyst, that is, b_o/a_o, exceeds 0.12064, or the ratio of the reaction rate of the decay reaction to the autocatalytic reaction exceeds 0.102268, or the ratio of the reaction rate of nonautocatalytic reaction to the autocatalytic reaction exceeds 0.0318.

The method used by Witmer et al. (1986) for determining the multiplicity of a single ODE has been extended to two ODE's. Furthermore, Liapunov-Schmidt procedure was used to analyze the two algebraic equations derived from the two ODE's. This computational method is easy to formulate and gives more accurate results than constructing bifurcation diagrams from parametric studies reported in the literature.

Notation

$a(Z)$ = concentration profile for species A
$b(Z)$ = concentration profile for species B
c = parameter value, Eq. 54
D_e = effective diffusivity
$\mathbf{F}$ = functions describing steady state
$G_1(w, \phi^2)$ = functions, Eq. 16
$G_2(w, \phi^2)$ = functions, Eq. 17
$G_3(w, \phi^2)$ = functions, Eq. 29
k_1 = reaction rate constant for autocatalytic reaction
k_u = reaction rate constant for nonautocatalytic reaction
k_d = reaction rate constant for decay reaction
L = half-thickness of catalytic slab
$\mathbf{L}$ = Jacobian matrix, Eq. 20
n = reaction order
p = parameter vectors, Eq. 15
$q_{ijk}(\xi, t)$ = sensitivity functions, Eqs. 22, 44
t = state variables, $X_A(0)$, $X_B(0)$
u = eigenvectors of Jacobian matrix, Eqs. 41
v = eigenrows of Jacobian matrix, Eq. 41
w = variables for initial value problems, Eqs. 16, 17
$X_A(\xi)$ = dimensionless concentration profile for species A
$X_B(\xi)$ = dimensionless concentration profile for species B
Z = coordinate

Greek letters

$\alpha = k_u/k_1 a_o^n$, Eq. 8
γ = parameters, Eq. 58
λ = bifurcation parameter, Eq. 58
$\sigma = b_o/a_o$, Eq. 8
ϕ = Thiele modulus, Eq. 8
ξ = dimensionless coordinate
$\delta = k_d/k_1 a_o^n$, Eq. 8
ϵ_i = parameters, Eq. 42

Subscript

o = surface conditions

Appendix A

Limit points for quadratic autocatalytic reactions with $\sigma = 0$ and $\alpha = 0$

Since no reaction takes place at point A, the limit points can be obtained by solving Eq. 20 with $w_1(\xi) = 1$ and $w_2(\xi) = 0$. By substitution of Eqs. 16 and 17 into Eqs. 23–26 with $\sigma = \alpha = 0$, we get

$$\frac{d^2q_{11}}{d\xi^2} = \phi^2 q_{21} \tag{A1}$$

$$\frac{d^2q_{12}}{d\xi^2} = \phi^2 q_{22} \tag{A2}$$

$$\frac{d^2q_{21}}{d\xi^2} = \phi^2(\delta - 1)q_{21} \tag{A3}$$

$$\frac{d^2q_{22}}{d\xi^2} = \phi^2(\delta - 1)q_{22} \tag{A4}$$

If $\delta > 1$, the solutions for Eqs. A1–A4 with initial conditions Eqs. 27 and 28 are

$$q_{11}(\zeta) = 1, \quad q_{12} = [\cosh \phi\sqrt{(\delta - 1)}\zeta - 1]/(\delta - 1)$$
$$q_{21}(\zeta) = 0, \quad q_{22} = \cosh \phi\sqrt{(\delta - 1)}\zeta \tag{A5}$$

Substituting Eq. A5 into Eq. 20, we get

$$\det \mathbf{L} = \cosh \phi\sqrt{(\delta - 1)} \tag{A6}$$

Since $\cosh x$ cannot be equal to zero, there is no limit point for $\delta > 1$.

If $\delta < 1$, the solutions are

$$q_{11}(\zeta) = 1, \quad q_{12} = [1 - \cos \phi\sqrt{(1 - \delta)}\zeta]/(1 - \delta)$$
$$q_{21}(\zeta) = 0, \quad q_{22} = \cos \phi\sqrt{(1 - \delta)}\zeta \tag{A7}$$

Substituting Eq. A7 into Eq. 20, we get

$$\det \mathbf{L} = \cos \phi\sqrt{(1 - \delta)} \tag{A8}$$

Thus, the limit point A occurs at

$$\phi\sqrt{(1 - \delta)} = \Pi/2 \tag{A9}$$

Appendix B

Initial value problem governing the sensitivity functions q_{ijk}

$$\frac{d^2q_{i11}}{d\xi^2} = \frac{\partial^2 gi}{\partial w_1^2} q_{11}^2 + 2\frac{\partial^2 G_i}{\partial w_1 \partial w_2} q_{11}q_{21} + \frac{\partial^2 G_i}{\partial w_2^2} q_{21}^2 + \frac{\partial G_i}{\partial w_{18}} q_{111} + \frac{\partial G_i}{\partial w_2} q_{211} \tag{B1}$$

$$\frac{d^2q_{i12}}{d\xi^2} = \frac{\partial^2 G_i}{\partial w_1^2} q_{11}q_{12} + \frac{\partial^2 G_i}{\partial w_1 \partial w_2} q_{21}q_{12} + \frac{\partial^2 G_i}{\partial w_2^2} q_{21}q_{22} + \frac{\partial^2 G_i}{\partial w_1 \partial w_2} q_{11}q_{22} + \frac{\partial G_i}{\partial w_1} q_{112} + \frac{\partial G_i}{\partial w_2} q_{212} \quad \text{(B2)}$$

$$\frac{d^2q_{i22}}{d\xi^2} = \frac{\partial^2 G_i}{\partial w_1^2} q_{12}^2 + 2\frac{\partial^2 G_i}{\partial w_1 \partial w_2} q_{12}q_{22} + \frac{\partial^2 G_i}{\partial w_2^2} q_{22}^2 + \frac{\partial G_i}{\partial w_1} q_{122} + \frac{\partial G_i}{\partial w_2} q_{222} \quad \text{(B3)}$$

for $i = 1, 2$ with initial conditions

$$q_{i11}(0) = q_{i12}(0) = q_{i22}(0) = 0 \quad \text{(B4)}$$

$$\frac{dq_{i11}}{d\xi}(0) = \frac{dq_{i12}}{d\xi}(0) = \frac{dq_{i22}}{d\xi}(0) = 0 \quad \text{(B5)}$$

Initial value problems governing the sensitivity functions q_{i3}

$$\frac{d^2q_{i3}}{d\xi^2} = \frac{\partial G_i}{\partial(\phi^2)} + \frac{\partial G_i}{\partial w_1} q_{13} + \frac{\partial G_i}{\partial w_2} q_{23} \quad \text{(B6)}$$

for $i = 1, 2$ with initial conditions

$$q_{13}(0) = q_{23}(0) = 0 \quad \text{(B7)}$$

$$\frac{dq_{13}}{d\xi}(0) = \frac{dq_{23}}{d\xi}(0) = 0 \quad \text{(B8)}$$

Initial value problems governing the sensitivity functions q_{ij3}

$$\frac{d^2q_{ij3}}{d\xi^2} = \frac{\partial^2 G_i}{\partial w_1^2} q_{1j}q_{13} + \frac{\partial^2 G_i}{\partial w_2 \partial w_2} q_{2j}q_{13} + \frac{\partial^2 G_i}{\partial w_2^2} q_{2j}q_{23} + \frac{\partial^2 G_i}{\partial w_1 \partial w_2} q_{1j}q_{23} + \frac{\partial G_i}{\partial w_1} q_{1j3} + \frac{\partial G_i}{\partial w_2} q_{2j3} + \frac{\partial^2 G_i}{\partial w_1 \partial \phi^2} q_{1j} + \frac{\partial^2 G_i}{\partial w_2 \partial \phi^2} q_{2j} \quad \text{(B9)}$$

for $i = 1, 2$ and $j = 1, 2$ with initial conditions

$$q_{ij3}(0) = \frac{dq_{ij3}}{d\xi}(0) = 0 \quad \text{(B10)}$$

Literature Cited

Aris, R., P. Gray, and S. K. Scott, "Modeling Cubic Autocatalysis by Successive Bimolecular Steps," *Chem. Eng. Sci.*, **43**(2), 207 (1988).

Balakotaiah, V., and D. Luss, "Structure of the Steady-State Solutions of Lumped-Parameter Chemically Reacting Systems," *Chem. Eng. Sci.*, **37**, 1611 (1982).

———, "Global Analysis of the Multiplicity Features of Multi-Reaction Lumped-Parameter Systems," *Chem. Eng. Sci.*, **39**, 865 (1984).

———, "Steady-State Multiplicity Features of Lumped-Parameter Chemically Reacting Systems," *Dynamics of Nonlinear Systems*, Gordon and Breach (1986).

Balakotaiah, V., D. Luss, and B. L. Keyfitz, "Steady-State Multiplicity Analysis of Lumped-Parameter Systems Described by a Set of Algebraic Equations," *Chem. Eng. Commun.*, **36**, 121 (1985).

Epstein, J. R., "Patterns in Time and Space—Generated by Chemistry," *Chem. Eng. News*, March 30, 24 (1987).

Golubitsky, M., and B. L. Keyfitz, "A Qualitative Study of the Steady-State Solutions for a Continuous Stirred Tank Reactor," *SIAM J. Math. Anal.*, **11**, 316 (1980).

Gray, P., and S. K. Scott, "Autocatalytic Reactions in the Isothermal Continuous, Stirred-Tank Reactor: Isola and Other Forms of Multiplicity," *Chem. Eng. Sci.*, **38**, 29 (1983).

———, "Autocatalytic Reactions in the Isothermal Continuous, Stirred-Tank Reactor: Oscillations and Instabilities in the System $A + 2B \rightarrow 3B$, $B \rightarrow C$," *Chem. Eng. Sci.*, **39**, 1087 (1984).

Hu, R., V. Balakotaiah, and D. Luss, "Multiplicity Features of Porous Catalytic Pellets. II: Influence of Reaction Order and Pellet Geometry," *Chem. Eng. Sci.*, **40**, 599 (1985).

Kaas-Petersen, C., and S. K. Scott, "Stationary-State and Hopf Bifurcation Patterns in Isothermal Reaction-Diffusion Systems," *Chem. Eng. Sci.*, **43**, 391 (1988).

Nicolis, G., and I. Prigogine, "Self-Organization in Nonequilibrium Systems," Wiley, New York (1977).

Sapre, A. V., "Interaction of Diffusion and Autocatalysis," AIChE Ann. Meet., Washington DC (1988).

———, "Diffusional Enhancement of Autocatalytic Reactions in Catalyst Particles," *AIChE J.* **35**(4), 655 (1989).

Scott, S. K., "Isola, Mushrooms, and Oscillations in Isothermal, Autocatalytic Reaction-Diffusion Equations," *Chem. Eng. Sci.*, **42**, 307 (1987).

Scott, S. K., and W. W. Farr, "Dynamic Fine Structure in the Cubic Autocatalator," *Chem. Eng. Sci.*, **43**, 1706 (1988).

Witmer, G. S., V. Balakotaiah, and D. Luss, "Multiplicity Features of Distributed Systems. I: Langmuir-Hinshelwood Reaction in a Porous Catalyst," *Chem. Eng. Sci.*, **41**, 179 (1986).

Manuscript received June 20, 1989, and revision received Dec. 18, 1989.